JOURNAL OF CATALYSIS 147, 417–428 (1994)

Silica–Alumina-Supported Acidic Molybdenum Catalysts—TPR and XRD Characterization

S. Rajagopal, H. J. Marini,[1] J. A. Marzari, and R. Miranda[2]

Department of Chemical Engineering, University of Louisville, Louisville, Kentucky 40292

Received May 24, 1993; revised December 20, 1993

A series of silica–aluminas with controlled composition has been synthesized and used as supports for Mo oxide catalysts. X-ray diffraction (XRD) and temperature-programmed reduction (TPR) were used to study the role of support composition upon the stability of various oxidic species, including products of solid state reaction between Mo oxide and silica–alumina. In general, the reducibility of Mo increases with increasing Mo loading, regardless of support composition. For a fixed Mo loading, however, extent of reduction increases with SiO_2 content and shows a maximum at a composition $SiO_2:Al_2O_3 = 75:25$ (wt%). Except for silica-rich catalysts, the average oxidation state of Mo does not reach below +4 at the conditions used for TPR (maximum temperature: 550°C). Most of the support compositions yield XRD-amorphous Mo oxide. Only Mo-rich and silica-rich catalysts ($MoO_3 \geq 12$ wt%; $SiO_2 \geq 50$ wt%) contain crystalline phases of Mo: orthorhombic MoO_3 on 100% SiO_2, and MoO_3 and $Al_2(MoO_4)_3$ on silica–aluminas. © 1994 Academic Press, Inc.

INTRODUCTION

The design and synthesis of catalysts containing supported transition metal oxides (TMO) demand adequate control of oxide dispersion, oxidation state, phase characteristics, and stability during treatment or utilization. As inferred from the work of Williams *et al.* (1), some supported oxide systems seem to reach structural and chemical equilibrium under typical preparation and utilization conditions. In those systems, control of microstructure or chemical state of the supported oxide may be hard to attain, as in the case of Mo oxide catalysts. Stable structural modifications of the supported TMO can be obtained, however, by affecting the nature of the support or by addition of promoters or chemical modifiers. In this work we report on the effect of composition of silica–alumina on the characteristics of supported Mo oxide. Although one of the main features of this support is the introduction of Brønsted acidity, in this paper we have focused on the characterization of Mo oxide reducibility and structural stability.

Reducibility of supported TMO is altered by the degree of TMO-support chemical interaction, which also affects the dispersion of the TMO and the character of the surface species formed during catalyst preparation and treatment. As documented in the literature, reducibility behavior can be readily studied via temperature-programmed reduction (TPR) (2, 3). This technique has been extensively applied to supported Mo oxide catalysts (4–27), encompassing various supports such as Al_2O_3 (4–24), SiO_2 (5, 12, 16, 19, 23–27), SiO_2–Al_2O_3 (4, 12, 19), TiO_2 (16), and MgO (16). The identity and TPR features of Mo species over Al_2O_3 and SiO_2 were characterized for the most part in the early works of Thomas *et al.* (5) and Hall (10). On Al_2O_3, Thomas *et al.* identified three different Mo species: octahedral (Mo_O), tetrahedral (Mo_T) (Raman absorption at 860 cm^{-1}), and an unnamed molybdate; on SiO_2 they found the same octahedral and tetrahedral species, and bulk MoO_3. On Al_2O_3, Hall confirmed the presence of polymeric clusters of octahedral Mo and smaller amounts of tetrahedral Mo. The TPR of Mo-oxides/Al_2O_3 was also studied by Yao (7), who observed that complete reduction of Mo to metal is possible at 900°C. TPR studies of Mo-oxides/SiO_2–Al_2O_3, however, are rare. In one such study, Brito and Laine (12) observed complex TPR patterns due to heterogeneity of surface Mo species. This heterogeneity could have been caused by the use of nonhomogenous silica–alumina supports, which were prepared by impregnating SiO_2 with $Al(NO_3)_3$, and by the use of H_2–N_2 as reduction gas, which could have nitrided the Mo.

Structural information of supported Mo oxides can be obtained with XRD. On SiO_2, Mo oxide yields a phase of orthorhombic MoO_3 even at loadings as low as 2.4 wt% (28). On Al_2O_3, Mo oxide forms X-ray amorphous monolayers or islands for surface concentration of Mo below 5 atoms nm^{-2} (9, 15). Above this concentration, XRD reveals the appearance of bulk crystalline MoO_3. XRD data of Mo oxide on amorphous silica–aluminas is scarce. Only recently have Henker *et al.* (29, 30) shown spectra of heavily loaded silica–aluminas, and found

[1] Present address: Facultad de Química, Univ. Nac de San Luis, 5800 San Luis, Argentina.

[2] To whom correspondence should be addressed.

0021-9517/94 $6.00

$Al_2(MoO_4)_3$ to be one of the crystalline phases present, in addition to MoO_3. Here, we are demonstrating for the first time that even low Mo loadings on "precalcined" silica–aluminas yield $Al_2(MoO_4)_3$.

None of the studies mentioned above showed an attempt to relate the composition of the supports with the structural and reducibility properties of the resultant Mo oxide catalysts. The aim of this publication is to fill such a void by providing quantitative TPR and XRD characterization of a comprehensive set of silica–alumina-supported Mo oxide catalysts, that were prepared under well-controlled and comparable conditions.

EXPERIMENTAL

Catalyst Synthesis

Al_2O_3 was prepared by first dissolving 375 g of $Al(NO_3)_3 \cdot 9H_2O$ (Fisher Scientific) in 1 liter of distilled water. A solution of 200 g of NaOH in 750 ml distilled water was added to the $Al(NO_3)_3$ solution at a rate such that no precipitation occurred during the addition. Fifty-five grams of HNO_3 in 500 ml of water was then added to the above $NaAlO_2$ solution at a rate of 1 ml min^{-1}, under mechanical stirring and at a constant temperature of 70°C. The addition of HNO_3 was continued until the pH reached 7.0. The suspension was filtered and washed with 2 liters of hot 1% NH_4NO_3 solution and 2 liters of distilled water.

The silica–aluminas ($SiO_2 : Al_2O_3$ weight ratios = 10 : 90, 25 : 75, 50 : 50, 75 : 25, and 90 : 10) were prepared according to established techniques (31). Required amounts of $Na_2SiO_3 \cdot 9H_2O$ were dissolved in distilled water to get a solution of pH 11.8. HNO_3 (3*N*) was added dropwise until the silicate solution gellified (pH 9.8). The gel was aged for 15 min at a temperature of 35°C.

A requisite amount of $Al(NO_3)_3 \cdot 9H_2O$ as demanded by the SiO_2/Al_2O_3 ratio was dissolved in distilled water and then mixed with the silica gel. The mixture was stirred for 10 min and 8 *N* NH_4OH was added dropwise until a pH of about 6 was reached. NH_4NO_3 solution was then added to the preparation and the pH was further increased from 6 to 7 using NH_4OH. The precipitate was aged for 2 h at 35°C and for 6 h at 45°C.

SiO_2 was obtained from $Na_2SiO_3 \cdot 9H_2O$ (Fisher Scientific) and 3*N* HNO_3 or H_2SO_4. All of the above solids were dried at 120°C for 4 h and calcined at 550°C for 12 h. The silica–alumina samples were ion exchanged three times with NH_4NO_3 and further calcined at 550°C. XRD of the powders revealed the amorphicity of SiO_2 and silica–aluminas with ≥50 wt% SiO_2. The alumina support was confirmed to be γ-Al_2O_3. The content of γ-Al_2O_3 decreases with increasing SiO_2, becoming negligible in silica–alumina of 50 wt% SiO_2. The synthesized supports are designated as Al_2O_3, SA10, SA25, SA50, SA75, SA90, and SiO_2, where Al_2O_3 stands for γ-Al_2O_3, SA10 for $SiO_2 : Al_2O_3$ = 10 : 90 wt%, SA25 for $SiO_2 : Al_2O_3$ = 25 : 75 wt%, etc.

Supported Mo oxide was prepared by incipient wetness (dry) impregnation with $(NH_4)_6\ Mo_7O_{24} \cdot 4H_2O$ (AHM) (Alfa Products). For this purpose, pore volume of the supports was determined by means of water titration. The resulting pore volumes in ml g^{-1} were: Al_2O_3 (1.0), SA10 (0.75), SA25 (0.80), SA50 (0.87), SA75 (0.87), SA90 (0.82), SiO_2 (0.97). The loading of Mo oxide on each support was varied in a range corresponding to theoretical submonolayer to monolayer coverage (2, 4, 8, and 12 wt% MoO_3). For this purpose, the required concentration and volume of aqueous AHM, at a pH around 5.8, was added to ≈4 g of the carrier at room temperature. Table 1 describes the actual concentration of Mo and pH of the AHM solutions used in the synthesis of MoO_3/Al_2O_3 catalysts. Similar conditions were used for the other catalysts. The impregnated samples were left at room temperature for 2 h before drying at 120°C for 6 h. Calcination was performed in air at 550°C for 12 h. Mo content in the final calcined catalysts was verified by X-ray fluorescence spectroscopy. The supported catalysts are designated as M2Al for 2 wt% MoO_3/Al_2O_3, M4SA90 for 4 wt% MoO_3/SA90, etc.

A reference sample of bulk MoO_3 was prepared as described in the literature (32). One gram of AHM was dissolved in a minimum amount of water and poured into 200 ml of ethanol. The precipitated AHM was filtered and dried to obtain a fine powder. Controlled heating up to 300°C at a rate of 100°C h^{-1}, and calcination at 500°C for 12 h, produced orthorhombic MoO_3 with a specific surface area of 3.2 $m^2\ g^{-1}$. Since some of the TPR experiments required a diluted bulk MoO_3 sample, a physical mixture containing 12 wt% MoO_3 was prepared using SiO_2 (311 $m^2\ g^{-1}$) as a diluent; this sample is designated as PM12Si. All of the samples were stored in desiccator for further use.

Surface Area

BET specific surface area (S_{BET}) of the 7 supports and 28 catalysts was determined by N_2 sorption at −196°C using a conventional all-glass vacuum apparatus equipped

TABLE 1

Concentration and pH of Impregnating Solutions during Preparation of MoO_3/Al_2O_3 Catalysts[a]

Catalyst	Mo (mg cm^{-3})	pH
2% MoO_3/Al_2O_3	13.60	5.4
4% MoO_3/Al_2O_3	27.77	5.7
8% MoO_3/Al_2O_3	57.96	5.9
12% MoO_3/Al_2O_3	90.89	6.1

[a] A similar procedure was utilized to prepare other supported catalysts.

TABLE 2

BET Surface Areas of Supports and Supported Mo Oxide Catalysts

Supports	BET surface area ($m^2\ g^{-1}$)				
	0% MoO_3	2% MoO_3	4% MoO_3	8% MoO_3	12% MoO_3
Al_2O_3	150	148	148	141	137
SA10	264	208	200	179	170
SA25	297	223	222	213	191
SA50	306	238	226	209	204
SA75	294	226	215	199	187
SA90	382	322	308	277	247
SiO_2	311	298	288	255	213

with an electronic manometer (Datametrics). The results are reported in Table 2. As expected, the calcined catalysts have less S_{BET} than the supports and show decreasing S_{BET} with increasing Mo loading. This is most evident for the silica–alumina supported catalysts. These changes are suspected to be caused by plugging of support pores due to agglomeration of Mo oxide. Solid state reactions leading to new phases are not believed to be responsible for the lower surface areas.

X-Ray Diffraction

About 40 mg of catalyst sample was supported in a zero-background holder. Powder diffraction spectra were obtained with a Rigaku diffractometer model D/Max-B using Ni-filtered Cu$K\alpha$ radiation at 40 kV and 35 mA. The reduced samples were exposed to air at room temperature before the XRD spectra were collected. Surface reoxidation of Mo was not expected to affect the XRD signature of any bulk crystalline phase formed.

TPR Studies

The TPR apparatus (Fig. 1) consisted of a quartz reactor (ID: 8 mm, sintered frit diameter: 6 mm) and a thermal conductivity detector (TCD) interfaced with an integrator (Hewlett–Packard). Heating was performed with a tubular furnace regulated by a soak-and-ramp temperature controller (Lindberg). The reducing gas consisted of a mixture of H_2 and Ar, which were purified by flow through "oxygen trap" and molecular sieves (Alltech Associates) to remove oxygen and water, respectively. Ar was preferred as a diluent gas over N_2 since Mo oxide is known to react with N_2 under TPR conditions to form nitrides (33, 34). The flow rate of individual gases was regulated by mass flow controllers (Datametrics) and the mixture was homogenized in a 100-ml stainless steel bulb. The water produced during reduction was condensed in a cold trap of dry ice and *n*-propanol.

The sample size in each TPR experiment was 40 μmol of Mo oxide, and was kept constant for all runs. Therefore

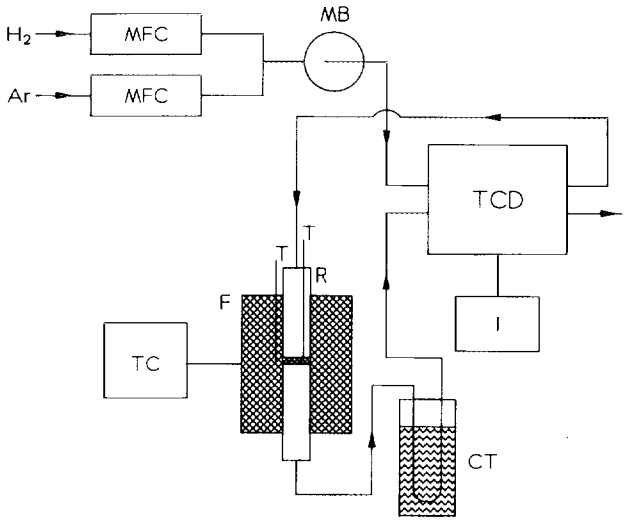

FIG. 1. Temperature programmed reduction unit. MFC, mass flow controllers; MB, mixing bulb; R, quartz reactor; T, type-K thermocouple; F, tubular furnace; TC, temperature controller; CT, cold trap; TCD, thermal conductivity detector; I, integrator.

the catalyst weight was varied according to Mo oxide loading: 288 mg (for 2 wt% MoO_3), 144 mg (for 4%), etc., in all cases resulting in a very shallow bed. Diffusion limitations were experimentally shown to be absent, since the TPR spectra were independent of weight and flow rate in the ranges used in this work. Before each run, the samples were pretreated in 30 ml min^{-1} flow of dry O_2 at 500°C for 1 h to remove adsorbed impurities. Then they were cooled to 50°C, reduced in 30 ml min^{-1} stream of 10% H_2 in Ar while ramping the temperature from 50 to 550°C at 10°C min^{-1}, and kept at 550°C for 30 min. A few representative samples were reduced up to 900°C. The known problematic volatility of bulk MoO_3 at 650°C (35) is obviated in TPR experiments since most of the free MoO_3 is reduced by the time the temperature reaches 550°C.

The H_2 concentration in the effluent stream was monitored with the TCD and the areas under the peaks were integrated to determine the H_2 consumed. Blank TPR experiments of all seven supports showed no H_2 uptake up to 900°C. Calibration of the TCD was performed by stoichiometrically reducing a known amount of high purity CuO to Cu, a method which was found to be more reliable and reproducible than sending known volumes of H_2 pulses through the reactor (36). The availability of high-purity CuO and its complete reduction to Cu in a single step (39–41) make this compound an appropriate material for this purpose. CuO (21) and V_2O_5 (37, 38) have earlier been used for calibrating TPR instruments.

The amount of H_2 consumed in each TPR run is expressed in terms of the change in the average oxidation number (ΔON) of Mo. For example, $\Delta ON = 2$ indicates an average reduction of MoO_3 to MoO_2, thus implying

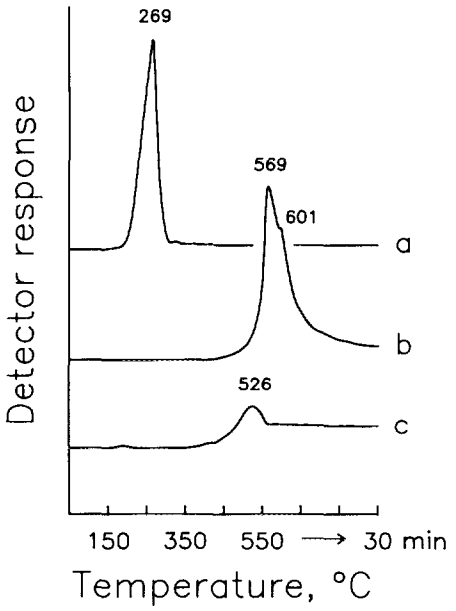

FIG. 2. TPR profiles of (a) CuO (20 μmol), (b) physical mixture of 12% MoO_3 in SiO_2, and (c) unsupported MoO_3 (40 μmol) prepared from ammonium heptamolybdate.

that H_2 consumption is exclusively due to the reduction of Mo. H_2 adsorption, as observed by Hall and Massoth (42), was not accounted for. This omission is not considered a serious drawback in the interpretation of our results.

The terms reducibility and extent of reduction, used in the text, are defined as follows. Reducibility of a pure phase is determined by the energy of activation for reduction, and thus is inversely related to the temperature at which reduction occurs. Extent of reduction of a supported Mo oxide catalyst is characterized in this work by the ΔON of Mo, and it depends on the amount and the reducibility of Mo species present, and on the experimental conditions of TPR.

RESULTS

Unsupported MoO_3

Figure 2 shows the TPR of reference CuO and bulk MoO_3. Since the sample size was set at 40 μmol Mo, the small amount of bulk MoO_3 (5.8 mg) had to be diluted with SiO_2 to avoid channeling and external diffusion limitations on the TPR spectra. It is observed that the diluted MoO_3 (PM12Si) is reduced substantially more (212%) than the undiluted one, justifying this procedure. Under the same conditions, the 20-μmol CuO reference was completely reduced to Cu metal below 350°C.

Influence of Mo Oxide Loading on Reducibility

Figure 3 shows the TPR spectra of the supported Mo oxide catalysts. The shape and maxima (T_{max}) of the profiles are strongly dependent on support composition and Mo oxide loading. All of the catalysts, except those over SiO_2, yielded a two-peak pattern. As Mo loading increases, the first T_{max} shifts to lower temperature, clearly indicating that the interaction of Mo oxide with the support decreases as loading increases, a result which is in agreement with various studies (7, 9, 22). We concur with Thomas *et al.* (9), who attributed the low-temperature peak to the reduction of multilayers of Mo oxide. Multilayers, however, must be distinguished from bulk Mo oxide, such as that present on SiO_2. Bulk Mo oxide interacts weakly with SiO_2 and displays a single high-temperature peak whose T_{max} does not shift with increasing loading. The presence of microcrystals of orthorhombic MoO_3 in the 12% MoO_3/SiO_2 catalysts was confirmed with XRD.

Silica-rich catalysts ($50 \leq SiO_2 < 100\%$) present features of both γ-Al_2O_3 and SiO_2-supported catalysts. The low-temperature peak reflects the reduction of interacting multilayers of Mo oxide, while the high-temperature peak is due to microcrystals of MoO_3 and $Al_2(MoO_4)_3$; the formation of the latter, as well as the assignment of the various Mo species, is discussed later. Table 3 shows the amount of H_2 uptake (μmol) and the corresponding ΔON calculated from the entire TPR spectra. Figure 4 displays the ΔON as a function of Mo loading, and demonstrates that extent of reduction increases monotonically with Mo loading and depends strongly on support composition. To explain these results, we speculate that for Al_2O_3, SA10, and SA25, an increase in Mo loading produces growth of multilayers of Mo oxide, as inferred from Fig. 3. For SA50, SA75, and SA90, increasing Mo loading is accommodated to a large extent in the form of microcrystals of MoO_3 and $Al_2(MoO_4)_3$, as Fig. 3 suggests.

Influence of Support Composition on Reducibility

Figure 5 shows the TPR data reorganized to emphasize the effect of support composition. The change in the TPR spectra with respect to support composition is indicative

TABLE 3

Change in Average Oxidation Number (ΔON) during TPR up to 550°C of Supported Mo Oxide Catalysts

Support	Change in oxidation number			
	2% MoO_3	4% MoO_3	8% MoO_3	12% MoO_3
Al_2O_3	0.70 (14.0)[a]	0.86 (17.2)	1.10 (22.0)	1.37 (27.4)
SA10	0.72 (14.4)	0.82 (16.4)	1.07 (21.4)	1.37 (27.4)
SA25	0.72 (14.4)	0.88 (17.6)	1.21 (24.2)	1.67 (33.4)
SA50	0.82 (16.4)	1.09 (21.8)	1.69 (33.8)	2.07 (41.4)
SA75	1.10 (22.0)	1.60 (32.0)	2.26 (45.2)	2.59 (51.8)
SA90	1.05 (21.0)	1.55 (31.0)	2.12 (41.4)	2.40 (48.0)
SiO_2	0.84 (16.8)	1.34 (26.8)	1.95 (39.0)	2.25 (45.0)

[a] The values in parentheses are H_2 uptakes in μmol of H_2 per 40 μmol MoO_3.

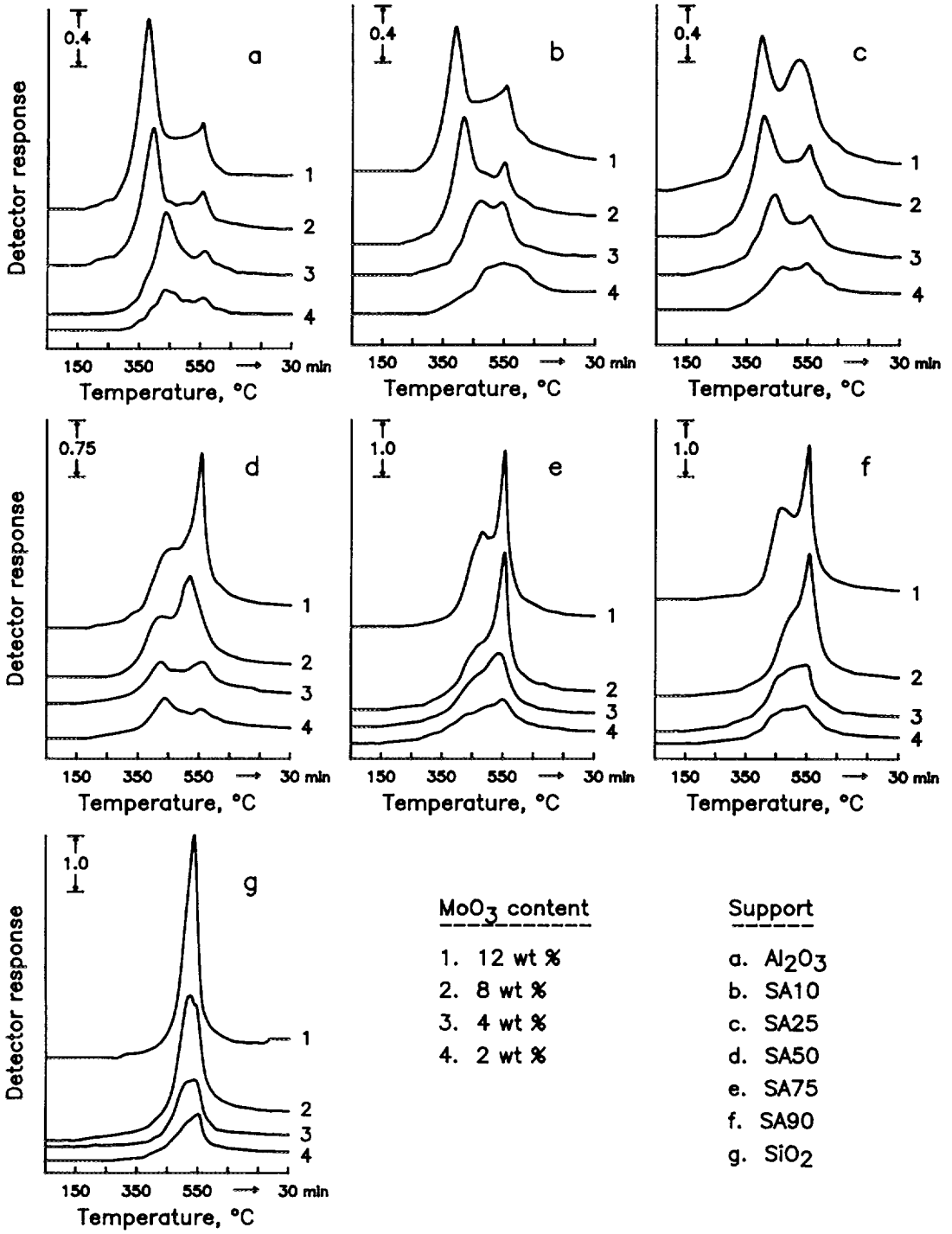

FIG. 3. TPR profiles of supported Mo oxide catalysts (40 μmol of Mo).

of the change in the type of predominant surface species. This figure reinforces the statement that Al_2O_3, SA10, and SA25 favor mainly the formation of polymolybdate or multilayered Mo oxide, while SA75 and SA90 favor mainly $Al_2(MoO_4)_3$ and microcrystalline MoO_3. SiO_2 support is unique in that it exhibits a single peak that indicates the homogeneity of MoO_3 microcrystals. This crystalline phase is less reducible than the multilayered oxide; therefore, it requires higher reduction temperature.

Figure 6 displays the ΔON as a function of support composition. The extent of reduction increases slowly up to 25% SiO_2 and rapidly beyond 50% SiO_2, showing an unexpected maximum at 75–80% SiO_2. The appearance of a maximum $\Delta ON = 2.6$ (average oxidation state of Mo

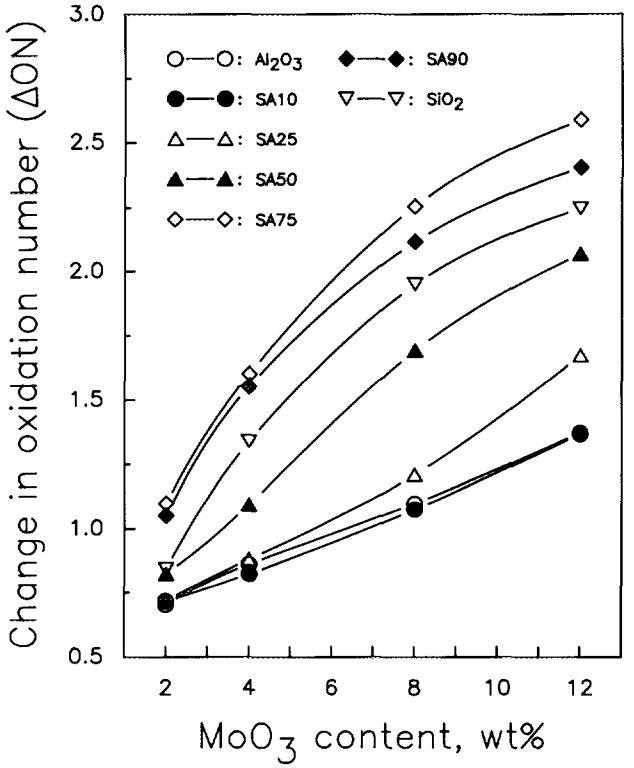

FIG. 4. Change in average oxidation number (ΔON) versus MoO_3 loading (2, 4, 8, and 12%).

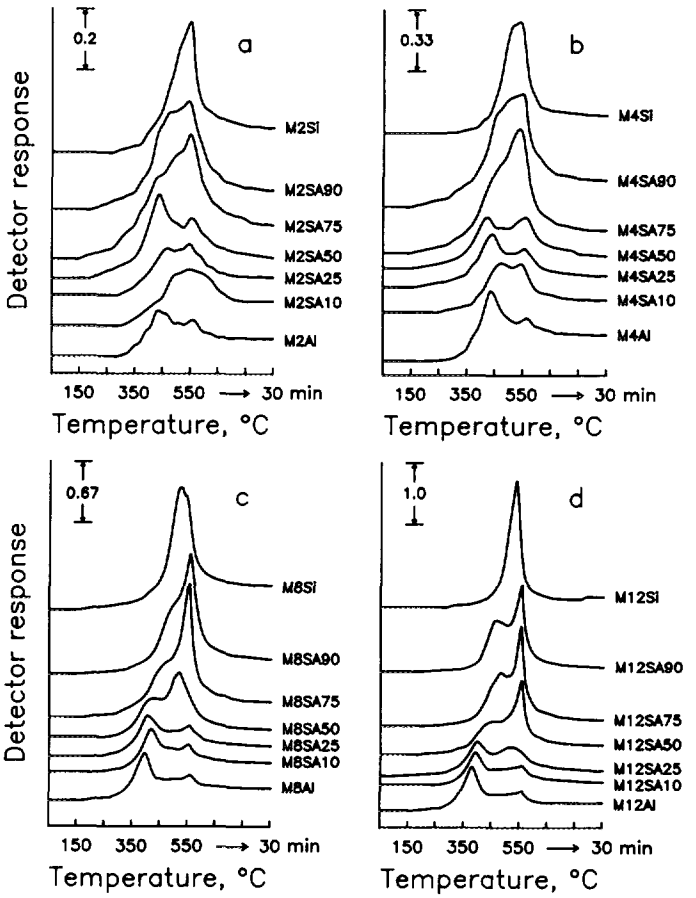

FIG. 5. TPR patterns of supported Mo oxide catalysts (40 μmol of Mo). (a) 2% MoO_3, (b) 4% MoO_3, (c) 8% MoO_3, and (d) 12% MoO_3.

= 3.4) is rationalized as follows. For a given Mo loading, as SiO_2 weight fraction increases, the interaction of Mo oxide with the support is reduced, and thus various Mo phases are generated, each one with characteristic reducibility. For example, it has already been shown that reducibility of $Al_2(MoO_4)_3$ is higher than that of orthorhombic MoO_3 (9). In the case of supports containing 75–80% SiO_2, Mo exists mainly as highly reducible Mo multilayers and $Al_2(MoO_4)_3$, some as crystalline MoO_3, and little as tetrahedrally coordinated species. This combination results in a maximum extent of reduction.

Figure 6 shows that, in the case of 2 and 4% MoO_3 samples, extent of reduction varies little for Al_2O_3 and alumina-rich supports. On those, enough alumina surface is available for Mo oxide to interact and form tetrahedral Mo species, which are difficult to reduce. For temperature up to 550°C, the reduction yields a $\Delta ON < 1$, that is, a Mo average oxidation state higher than 5.

TPR up to 900°C

Selected catalysts (M4Al, M12Al, M4SA75, M12SA75, M4Si, M12Si, and physical mixture PM12Si) were reduced up to 900°C. Figure 7 displays the known stepwise reduction of bulk MoO_3, i.e. $MoO_3 \rightarrow MoO_2 \rightarrow Mo$ (37, 43), which is confirmed by a ratio of areas under the peaks of approximately 1 : 2. Figure 8 shows analogous patterns

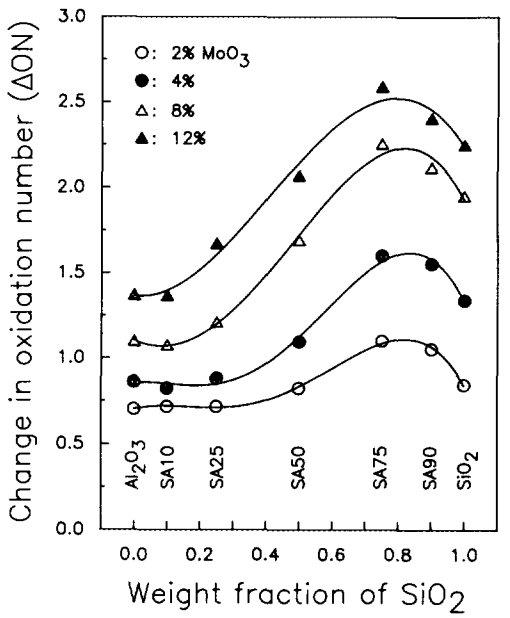

FIG. 6. Change in average oxidation number (ΔON) versus support composition in terms of weight fraction of SiO_2 in silica–alumina.

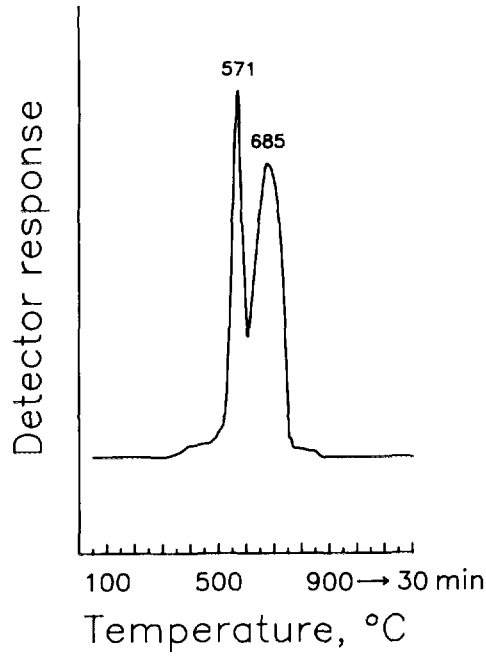

FIG. 7. TPR profile of physical mixture of 12% MoO_3 in SiO_2 (50–900°C).

for supported M4Si and M12Si, although in these cases the ratio of areas under the peaks is not 1 : 2, and thus the two peaks no longer represent exactly the two-step reduction suffered by bulk MoO_3. Both M4Si and M12Si are reduced to similar extents (Table 4), but the TPR

TABLE 4

Change in Average Oxidation Number (ΔON) during TPR up to 900°C of Mo Oxide Supported on SiO_2, Al_2O_3, and SiO_2–Al_2O_3

Sample	Designation	H_2 uptake[a]	ΔON
4% MoO_3/SiO_2	M4Si	106	5.3
12% MoO_3/SiO_2	M12Si	110	5.5
4% MoO_3/Al_2O_3	M4Al	112	5.6
12% MoO_3/Al_2O_3	M12Al	110	5.5
4% MoO_3/SA75	M4SA75	108	5.4
12% MoO_3/SA75	M12SA75	116	5.8
12% MoO_3 + 88% SiO_2[b]	PM12Si	118	5.9

[a] Hydrogen uptake in μmol of H_2 per 40 μmol MoO_3.
[b] Physical mixture of MoO_3 and SiO_2.

spectra differ in shape, a difference which is caused by the higher stability of MoO_3 on M4Si than on M12Si. A likely explanation for this stability is that the smaller crystallites present in M4Si are more interactive than the larger crystallites in M12Si. Diffusion limitation can be ruled out as a cause of change in the TPR shape, because such phenomenon would cause a similar shift in both T_{max}.

The TPR profiles of the γ-Al_2O_3-supported M4Al and M12Al catalysts are shown in Fig. 9. Both loadings display the same extent of reduction (Table 4), although the stability of M4Al is higher than that of M12Al. More clearly in this case than in the case of SiO_2 support, the relative changes in peak shape can be associated with changes in the type of Mo species undergoing reduction. The low-

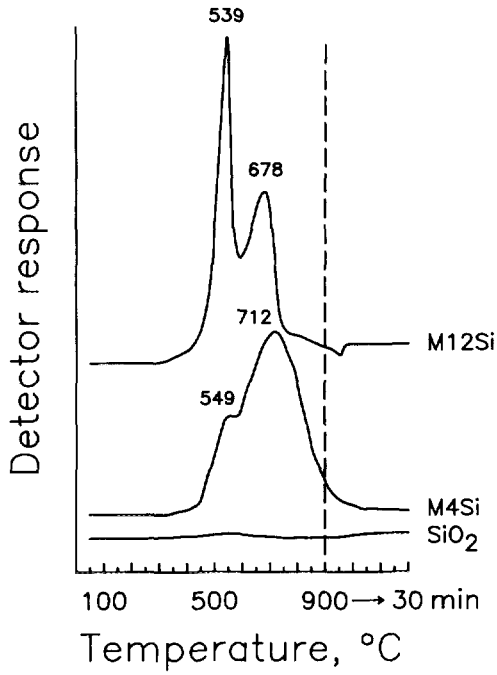

FIG. 8. TPR patterns of SiO_2-supported Mo oxide catalysts (50–900°C).

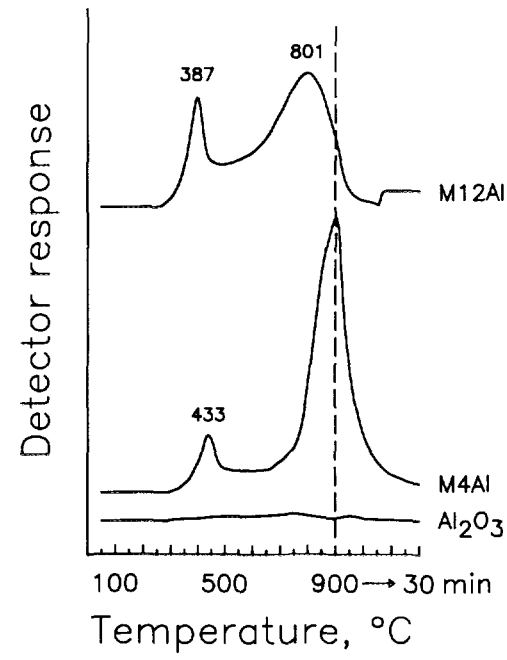

FIG. 9. TPR patterns of Al_2O_3-supported Mo oxide catalysts (50–900°C).

temperature peak can be assigned to the partial reduction ($Mo^{6+} \rightarrow Mo^{4+}$) of amorphous, highly defective, multilayered Mo oxides. The high-temperature peak encompasses the deep reduction of all Mo species, including highly dispersed Mo_T, multilayers of amorphous Mo oxides, and microcrystalline MoO_3. Thus, the larger relative area and T_{max} of the high-temperature peak in M4Al suggests that M4Al contains a larger fraction of dispersed Mo_T than M12Al. Correspondingly, M12Al contains a larger fraction of multilayered Mo oxides.

The TPR patterns of the silica–alumina-supported M4SA75 and M12SA75 catalysts (Fig. 10) are a composite of those of the SiO_2 and Al_2O_3 counterparts. For example, M4SA75 displays three peaks: a lower one suggesting the presence of multilayers of amorphous Mo oxides, and two higher ones that resemble the TPR of M4Si and suggest the presence of crystalline Mo species. This assignment is verified by the TPR pattern of M12SA75, with two central peaks resembling the M12Si spectrum, a lower peak corresponding to amorphous Mo oxides, and a high-temperature peak that resembles M12Al.

X-Ray Diffraction

XRD of the oxidic catalysts reveal that crystalline Mo species are present only in the high-silica 12% MoO_3 catalysts; M12SA50, M12SA75, M12SA90, and M12Si, although since the crystallite size detection limits is around 4 nm, smaller crystalline agglomerates may still be present in the other materials. Al_2O_3 and alumina-rich samples exhibit diffraction line characteristics of γ-Al_2O_3. XRD of the reduced catalysts shows that all phases of Mo become either amorphous or of short-range crystallinity.

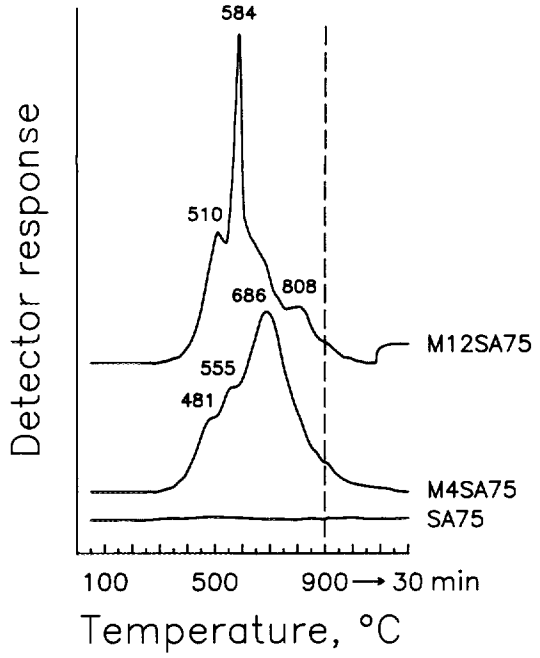

FIG. 10. TPR patterns of SA75-supported Mo oxide catalysts (50–900°C).

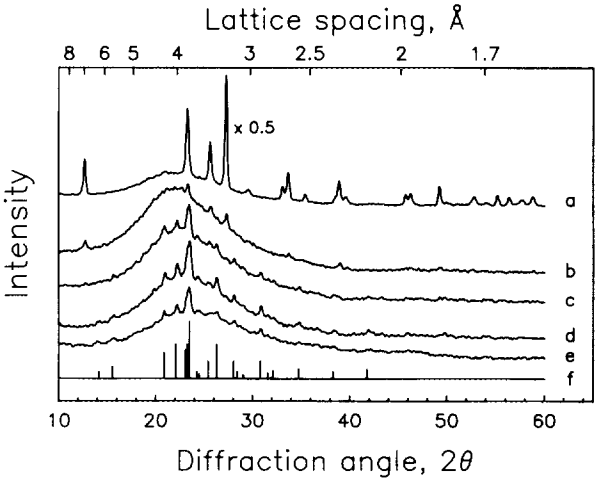

FIG. 11. XRD patterns of supported Mo oxide catalysts. (a) Physical mixture of 12% MoO_3 in SiO_2, (b) M12Si, (c) M12SA90, (d) M12SA75, (e) M12SA50, and (f) JCPDS card file 23-0764, which corresponds to $Al_2(MoO_4)_3$.

Figure 11 displays the XRD pattern of the four catalysts mentioned above and that of physical mixture PM12Si. Orthorhombic MoO_3 is detected on SiO_2, SA50, SA75, and SA90, while $Al_2(MoO_4)_3$ is formed only on silica-rich supports. From the intensity values it is found that the amount of $Al_2(MoO_4)_3$ formed is maximum at SA75. As evidenced in the published literature, the onset of crystalline phases of Mo oxide occurs at loadings that depend on the surface area of support, method of preparation, and thermal treatment. Recently, Datta *et al.* have tabulated published data (XRD, TEM, TPR, XPS, and Raman) on MoO_3/SiO_2 which show that the loading at which bulk MoO_3 phases begin to form varies widely (from 2.4 to 13%, according to XRD) (44).

DISCUSSION

It has been reported that Mo species are present in both octahedral (Mo_O) and tetrahedral (Mo_T) coordination when supported on SiO_2 and Al_2O_3, and as microcrystals of MoO_3 on SiO_2 (45). The nature of Mo oxide supported on silica–aluminas, however, has not been widely studied. In order to theorize on this point, it is relevant to review the adsorption behavior of AHM on SiO_2 and γ-Al_2O_3, and then to extrapolate it to amorphous silica–aluminas. In particular, the following aspects need to be qualified: (i) amount and basicity of OH groups present on the supports, (ii) mode of binding of Mo oxide precursors to OH groups during impregnation, and (iii) transformation of surface species during drying and calcination.

Various researchers have estimated the amount of basic and nonbasic OH groups present on SiO_2, γ-Al_2O_3, and silica–aluminas, using different techniques such as F-exchange, D_2 exchange, and NMR. Literature results are gathered and organized in Table 5. Although the absolute values vary from laboratory to laboratory, in any series of silica–aluminas the amount and density of basic OH groups decrease with increasing SiO_2 content. Correspondingly, the isoelectric point (IEP) of the solid varies smoothly between about 8 for Al_2O_3 to about 2 for SiO_2 (52, 53). In the present work, the impregnation solution had an initial pH between 5.4 and 6.1, depending on the concentration of Mo. That pH corresponds approximately to the IEP of SA50, as inferred from the published data (e.g., Ref. (52) reports an IEP of 6.4 for SA52). Thus, alumina-rich supports (Al_2O_3, SA10, and SA25) present a positively charged surface to the adsorbing species, while silica-rich supports (SA75, SA90, and SiO_2) have a negatively charged surface. The AHM solution contains MoO_4^{2-} and $Mo_7O_{24}^{6-}$ in equilibrium, and thus alumina-rich supports will strongly chemisorb both types of anion. These anionic species, however, will not be strongly chemisorbed by the silica-rich supports, and they will possibly deposit as clusters during the impregnation. Moreover, when the concentration of the AHM is high, as required for high metal loadings, a considerable amount of Mo remains in solution. Upon drying and calcination, the Mo in solution will precipitate to form multilayers of polymolybdates.

TABLE 5

The Surface Concentration of OH Groups on Al_2O_3, SiO_2, and Silica–Aluminas Determined by Various Investigators[a]

Sample	Surface area ($m^2\ g^{-1}$)	OH groups ($\mu mol\ m^{-2}$)	Method used	Ref.
γ-Al_2O_3	209	9.09[b]	F- exchange	46
SA10	331	6.98[b]	F- exchange	46
SA25	416	6.13[b]	F- exchange	46
SA75	425	4.38[b]	F- exchange	46
SiO_2	300	1.27[b]	F- exchange	46
γ-Al_2O_3	188	3.56	F- exchange	47
SA87	100	1.99	F- exchange	47
SiO_2	123	1.93	F- exchange	47
γ-Al_2O_3	250	3.0	$MoO_2(acac)_2$	22
γ-Al_2O_3	192	3.8[c]	NMR	48
γ-Al_2O_3	192	6.0[c]	D_2 exchange	48
γ-Al_2O_3	163	2.8	F- exchange	14
γ-Al_2O_3	175	4.6	Et_3Al	49
Al_2O_3	313	2.4[e]	F- exchange	50
SA10[d]	238	3.15[e]	F- exchange	50
SA20[d]	279	2.72[e]	F- exchange	50
SA40[d]	193	3.68[e]	F- exchange	50
SA60[d]	172	3.9[e]	F- exchange	50
SA80[d]	245	1.51[e]	F- exchange	50
SA90[d]	238	2.40[e]	F- exchange	50
SiO_2	242	0.41[e]	F- exchange	50
Al_2O_3	571	5.15[f]	NMR	51
SA10	768	5.65[f]	NMR	51
SA25	839	3.99[f] (0.33)[g]	NMR	51
SA50	727	4.48[f] (1.66)[g]	NMR	51
SA75	615	(1.99)[g]	NMR	51
SA90	693	(2.49)[g]	NMR	51
SiO_2	576	(2.66)[g]	NMR	51

[a] The reported values were converted to $\mu mol\ m^{-2}$ for easy comparison.

[b] *Active* OH concentration.

[c] Pretreatment temperature is 500°C.

[d] The value represents mol% SiO_2.

[e] According to Ref. (50), the surface OH groups measured by the F-exchange method are probably anionic.

[f] AlOH groups, 500°C calcined samples.

[g] SiOH groups, 500°C calcined samples.

On pure Al_2O_3, which contains mostly basic and some neutral and weakly acidic OH groups, the basic OH groups react preferentially with MoO_4^{2-} ions, while the neutral or weakly acidic OH groups react with $Mo_7O_{24}^{6-}$, as observed with IR spectroscopy (22, 54). It is known that for low loading, much of the deposited Mo oxide acquires tetrahedral coordination, and survives calcination in a highly dispersed state. Okamoto and Imanaka reported that tetrahedral coordination is maintained for density $< 10^{14}$ Mo atoms cm^{-2}, which corresponds to 3.5 wt% MoO_3 for the Al_2O_3 they used as support (15). Therefore, a large fraction of Mo species present in our 2 wt% MoO_3/Al_2O_3 catalysts is believed to be tetrahedrally coordinated (Mo_T). This argument provides a basis for our assignment of the second TPR peak in Fig. 3a to Mo_T. The low reducibility of this kind of species explains the low extent of reduction (Fig. 4), as well as the absence of XRD structure observed for these catalysts. The similarity of the TPR spectra of the 2 and 4 wt% catalysts allows us to infer that SiO_2 in contents up to 25% leaves enough density of basic OH groups to bind a large fraction of Mo as Mo_T.

Heptamolybdate ions attaching to neutral or slightly acidic OH groups probably do not retain their identity upon calcination and form multilayers of Mo oxide, anchored to the support through Mo–O–Al bonds. Earlier findings using Raman spectroscopy show that these multilayers of octahedrally coordinated Mo_O grow as Mo loading is increased (55). These findings are consistent with our assignment of the first TPR peak to multilayers of octahedrally coordinated species (Fig. 3). The reducibility of these species is higher than that of Mo_T species because of weaker interaction with the support, leading to the low T_{max} observed in Figs. 3a–3c. Furthermore, the reducibility of second and higher layers of Mo is greater than that of the first layer which is in contact with the support, explaining the observation made in Figs. 3a–3c that the first peak not only increases in size but also shifts to lower temperature with increasing Mo loading. It

must also be noted that these multilayers are X-ray amorphous.

SiO_2 surfaces contain OH groups which are less reactive than those on Al_2O_3. Their neutrality or weak acidity (IEP of SiO_2 is about 2) determines their poor capacity for adsorption of anionic Mo species. Weak interaction during impregnation results in loss of dispersion of SiO_2-supported Mo species upon drying and calcination, leading to crystallization of Mo oxides (Fig. 11b). Mo–O–Si bonds do not form readily at moderate temperatures; however, some dispersion by thermal spreading is likely to occur, as suggested by the TPR shown in Fig. 3g. The smaller crystallites, which are present on the less loaded catalysts, are reduced to a lesser extent than the larger crystallites. This can be explained by the stabilization of the Mo oxide crystallites provided by bonding to SiO_2 (56).

Amorphous silica–aluminas offer a surface chemistry of intermediate nature between that of SiO_2 and Al_2O_3. As the percentage of SiO_2 is increased, the OH density and basicity of the silica–alumina decrease (Table 5). Therefore, for a given loading, Mo may be distributed among several types of species, such as Mo_T, multilayers of amorphous Mo oxide, and crystalline phases. Alumina-rich (basic-OH rich) supports contain largely Mo_T and multilayers, while silica-rich supports contain mostly multilayers and crystalline phases. This scenario explains the two-peak low-temperature TPR pattern obtained for most of the silica–alumina-supported catalysts (Figs. 3b–3f). The first peak corresponds to the reduction of amorphous multilayers of Mo oxide and thus its area is correlated with the weight fraction of Al_2O_3. The second peak corresponds to the reduction of crystalline $Al_2(MoO_4)_3$ and MoO_3, and its area is correlated with the amount of SiO_2 in the support.

Formation of $Al_2(MoO_4)_3$

$Al_2(MoO_4)_3$, a thermodynamically stable phase, does not form when Mo oxide/γ-Al_2O_3 catalysts are calcined at usual temperature of 500–550°C. However, this phase has been reported to form in highly loaded catalysts at >720°C (55, 57, 58). The proposed mechanisms involves Mo^{6+} that incorporates into octahedral interstices of bulk spinel γ-Al_2O_3. This reaction is kinetically limited, as observed by Kasztelan *et al.* (59) with Raman spectroscopy when 14 wt% MoO_3/Al_2O_3 was calcined at 900°C.

Solid-state reaction between MoO_3 and silica–aluminas resulting in new phases is not anticipated to occur at 550°C. Massoth *et al.* (46) have reported XRD of silica–alumina-supported Mo catalysts, M12SA10, M12SA25, and M12SA75, which were synthesized by incipient wetness impregnation and calcined at 540°C. The supports were obtained from commercial sources. They found no crystalline Mo phases on M12SA10 and M12SA25, in accordance with our findings. However, they described a Mo phase on M12SA75 as MoO_3(?). It is not certain what they meant by the question mark: either that the diffraction lines were not exactly similar to those of crystalline MoO_3, or that they were too weak to be designated as MoO_3.

Recently, Henker *et al.* (30) have shown that MoO_3/SiO_2–Al_2O_3 catalysts prepared from *uncalcined* silica–aluminas that were ion exchanged with ammonium ion and impregnated with AHM at pH 10 yielded a new crystalline phase when calcined at 497°C for 2 h. That phase was identified by XRD as $Al_2(MoO_4)_3$. This appeared in four of the many compositions Henker *et al.* examined: M23SA20, M13SA43, M28SA43, and M31SA78, which range in SiO_2 content from 20 to 78 wt% and in MoO_3 loading from 13 to 31 wt%. The authors explained the unusual formation of $Al_2(MoO_4)_3$ by proposing that, during calcination of the AHM-impregnated *uncalcined* silica–aluminas, a large fraction of the tetrahedral Al is removed from the aluminosilicate, yielding highly reactive "extra-lattice" aluminum species. These species combine with Mo oxide at low temperature to form $Al_2(MoO_4)_3$. They also reported that $Al_2(MoO_4)_3$ is not formed when a precalcined silica–alumina is used (19). In that case, they contend that the extra-framework alumina is stabilized and hence not reactive enough to react with Mo oxide at low calcination temperature (550°C).

In the present work we report on the formation of $Al_2(MoO_4)_3$ at relatively low loading of Mo (12 wt% MoO_3) on silica–aluminas with SiO_2 content between 50 and 90 wt%, and under normal calcination conditions. Thus, it is shown for the first time that even precalcined silica–aluminas react with Mo species to form $Al_2(MoO_4)_3$ at 550°C. A possible explanation for this low-temperature reaction can be inferred from recent evidence showing that in amorphous silica–aluminas with $\geq$50 wt% SiO_2, only 20% of Al is tetrahedral and the rest is octahedral (60). This octahedral Al may actually form a dispersed alumina phase (as verified by the absence of XRD peaks) which is highly reactive and yields $Al_2(MoO_4)_3$ during calcination in the presence of Mo oxide. The occurrence of the well-known and mobile $MoO_2(OH)_2$ species, which is formed by reaction of MoO_3 and H_2O vapor at calcination temperature (61), would facilitate the diffusion of Mo species and growth of the molybdate phase.

The relatively long calcination time (12 h) used in the present study may also have helped this slow reaction. The $Al_2(MoO_4)_3$ phase is XRD detectable in the 12 wt% MoO_3 samples, but is likely to exist also in the 8 wt% catalysts, as indicated by the analogous TPR profiles and high extent of reduction observed for both loadings. The absence of $Al_2(MoO_4)_3$ in alumina-rich catalysts is consistent with the high OH density available to disperse the Mo species.

It may be noted that, contrary to Henker *et al.*, we did not observe formation of $Al_2(MoO_4)_3$ on SA20. In their case, the high pH ($\approx$10) of the impregnating solution, the *uncalcined* state of the silica-aluminas, and the high metal loading (23% MoO_3) may have contributed to compound formation on SA20. Their experimental conditions were almost equivalent to those used for catalysts preparation by coprecipitation. At pH 10, Al_2O_3 is known to be dissolved and form $Al(OH)_4^-$ (62). In fact, we also observed the almost quantitative formation of $Al_2(MoO_4)_3$ when a mixture of $Al(NO_3)_3$ and AHM solutions was lyophilized, dried, and calcined at 500°C.

CONCLUSIONS

Al_2O_3 and alumina-rich supports interact strongly with Mo oxide species due to the abundance of basic OH groups. Low loading ($MoO_3 \leq 4$ wt%) favors tetrahedral Mo species, which have low reducibility. High loading, on the other hand, promotes octahedral, multilayered Mo species, which have high reducibility and thus are characterized by a low-temperature TPR peak. The overall extent of reduction of alumina-rich catalysts, however, is much less than that of silica-rich counterparts. SiO_2 and silica-rich supports promote agglomeration of Mo oxide because of weak interaction, although some degree of dispersion of Mo oxide by SiO_2 is apparent. Upon calcination, SiO_2 carrier leads to a single crystalline phase equivalent to orthorhombic MoO_3, and silica-rich supports produce mainly three types of species: a multilayered Mo species characterized by a low-temperature TPR peak, a crystalline phase of orthorhombic MoO_3, and a crystalline phase of $Al_2(MoO_4)_3$ at high Mo loading ($MoO_3 \geq 12$ wt%). The crystalline phases are characterized by a high-temperature TPR peak. The formation of $Al_2(MoO_4)_3$ may be due to the presence of reactive and highly dispersed alumina, which reacts with Mo species upon calcination at 550°C.

ACKNOWLEDGMENTS

Financial support from DOE (Grant DE-FG22-89PC89771), NSF (Grant RII-8610671), and the Commonwealth of Kentucky (EPSCoR Office) is greatly appreciated.

REFERENCES

1. Williams, C. C., Ekerdt, J. C., Jehng, J. M., Hardcastle, F. D., and Wachs, I. E., *J. Phys. Chem.* **95,** 8791 (1991).
2. Hurst, N. W., Gentry, S. J., Jones, A., and McNicol, B. D., *Catal. Rev.* **24,** 233 (1982).
3. Jones, A., and McNicol, B. D., "Temperature Programmed Reduction for Solid Materials Characterization." Dekker, New York, 1986.
4. Holm, V. C. F., and Clark, A., *J. Catal.* **11,** 305 (1968).
5. Thomas, R., Mittelmeijer-Hazeleger, M. C., Kerkhof, F. P. J. M., Moulijn, J. A., Medema, J., and de Beer, V. H. J., *in* "Proceedings of the 3rd Climax International Conference on the Chemistry and Uses of Molybdenum" (H. F. Barry and P. C. H. Mitchell, Eds.), p. 85. Climax Molybdenum, Ann Arbor, MI, 1979.
6. Gajardo, P., Grange, P., and Delmon, B., *J. Chem. Soc., Faraday Trans. 1* **76,** 929 (1980).
7. Yao, H. C., *J. Catal.* **70,** 440 (1981).
8. Thomas, R., de Beer, V. H. J., and Moulijn, J. A., *Bull. Soc. Chim. Belg.* **90,** 1349 (1981).
9. Thomas, R., van Oers, E. M., de Beer, V. H. J., Madema, J., and Moulijn, J. A., *J. Catal.* **76,** 241 (1982).
10. Hall, K. W., *in* "Proceedings of the 4th Climax International Conference on the Chemistry and Uses of Molybdenum" (H. F. Barry and P. C. H. Mitchell, Eds.), p. 224. Climax Molybdenum, Golden, Colorado, 1982.
11. Cáceres, C. A., Fierro, J. L. G., López Agudo, A., Blanco, M. N., and Thomas, H. S., *J. Catal.* **95,** 501 (1985).
12. Brito, J., and Laine, J., *Polyhedron* **5,** 179 (1986).
13. van Veen, J. A. R., and Hendriks, P. A. J. M., *Polyhedron* **5,** 75 (1986).
14. Okamoto, Y., and Imanaka, T., *in* "Acid–Base Catalysis" (K. Tanabe, H. Hattori, T. Yamaguchi, and T. Tanaka, Eds.), p. 223. Proceedings of the International Symposium on Acid-Base Catalysis, Sapporo, Japan, 1988.
15. Okamoto, Y., and Imanaka, T., *J. Phys. Chem.* **92,** 7102 (1988).
16. Shimada, H., Sato, T., Yoshimura, Y., Hiraishi, J., and Nishijima, A., *J. Catal.* **110,** 275 (1988).
17. Kadkhodayan, A., and Brenner, A., *J. Catal.* **117,** 311 (1989).
18. López Cordero, R., Esquivel, N., Lázaro, J., Fierro, J. L. G., and López Agudo, A., *Appl. Catal.* **48,** 341 (1989).
19. Valyon, J., Henker, M., and Wendlandt, K.-P., *React. Kinet. Catal. Lett.* **38,** 265 (1989).
20. Sajkowski, D. J., Miller, J. T., Zajac, G. W., Morrison, T. I., Chen, H., and Fazzini, D. R., *Appl. Catal.* **62,** 205 (1990).
21. Mangnus, P. J., van Veen, J. A. R., Eijsbouts, S., de Beer, V. H. J., and Moulijn, J. A., *Appl. Catal.* **61,** 99 (1990).
22. van Veen, J. A. R., Hendriks, P. A. J. M., and Andrea, R. R., *J. Phys. Chem.* **94,** 5275 (1990).
23. López Cordero, R., Gil Llambias, F. J., and López Agudo, A., *Appl. Catal.* **74,** 125 (1991).
24. Ismail, H. M., Zaki, M. I., Bond, G. C., and Shukri, R., *Appl. Catal.* **72,** L1 (1991).
25. Thomas, R., van Oers, E. M., de Beer, V. H. J., and Moulijn, J. A., *J. Catal.* **84,** 275 (1983).
26. Biermann, J. J. P., Janssen, F. J. J. G., de Boer, M., van Dillen, A. J., Geus, J. W., and Vogt, E. T. C., *J. Mol. Catal.* **60,** 229 (1990).
27. Liu, T.-C., and Chang, C.-S., *J. Chin. Inst. Chem. Eng.* **22,** 285 (1991).
28. Ono, T., Anpo, M., and Kubokawa, Y., *J. Phys. Chem.* **90,** 4780 (1986).
29. Henker, M., Wendlandt, K.-P., Spiro, E. S., and Tkachenko, O. P., *Appl. Catal.* **61,** 353 (1990).
30. Henker, M., Wendlandt, K.-P., Valyon, J., and Bornmann, P., *Appl. Catal.* **69,** 205 (1991).
31. Magee, J. S., and Blazek, J. J., *in* "Zeolite Chemistry and Catalysis" (J. B. Rabo, Ed.), ACS Monograph 171, p. 615. ACS, Washington, DC, 1976.
32. Tsigdinos, G. A., and Swanson, W. W., *Ind. Eng. Chem. Prod. Res. Dev.* **17,** 208 (1978).
33. Hegedüs, A. J., Sasvári, K., and Neugebauer, J., *Z. Anorg. Allg. Chem.* **293,** 56 (1957).
34. Hillis, M. R., Kemball, C., and Roberts, M. W., *Trans. Faraday Soc.* **62,** 3570 (1966).
35. Samsonov G. V., "The Oxide Handbook." IFI/Plenum, New York, 1973.

36. Rajagopal, S., and Miranda, R., unpublished results.
37. Arnoldy, P., de Jonge, J. C. M., and Moulijn, J. A., *J. Phys. Chem.* **89,** 4517 (1985).
38. Cordero, R. L., Esquivel, N., Lázaro, J., Fierro, J. L. G., and Agudo, A. L., *Appl. Catal.* **48,** 341 (1989).
39. Gentry, S. J., Hurst, N. W., and Jones, A., *J. Chem. Soc., Faraday Trans. 1* **77,** 603 (1981).
40. Bedford, M., Purves, J. H., Self, V. A., and Sermon, P. A., *Appl. Catal.* **58,** 147 (1990).
41. Boyce, A. L., Graville, P. A., Sermon, P. A., and Vong, M. S. W., *React. Kinet. Catal. Lett.* **44,** 1 (1991).
42. Hall, W. K., and Massoth, F. E., *J. Catal.* **34,** 41 (1974).
43. Brito, J., Laine, J., and Pratt, K. C., *J. Mater. Sci.* **24,** 425 (1989).
44. Datta, A. K., Ha, J.-W., and Regalbuto, J. R., *J. Catal.* **133,** 55 (1992).
45. Massoth, F. E., *Adv. Catal.* **27,** 265 (1978).
46. Massoth, F. E., Muralidhar, G., and Shabtai, J., *J. Catal.* **85,** 53 (1984).
47. Cáceres, C. V., Fierro, J. L. G., Lázaro, J., Agudo, A. L., and Soria, J., *J. Catal.* **122,** 113 (1990).
48. Cirillo, Jr. A. C., Dollish, F. R., and Hall, W. K., *J. Catal.* **62,** 379 (1980).
49. Mariette, L., Hemidy, J. F., and Carnet, D., *in* "Adsorption and Catalysis on Oxide Surfaces" (M. Che and G. C. Bond, Eds.), p. 263. Elsevier, Amsterdam, 1985.
50. Yamagata, N., Owada, Y., Okazaki, S., and Tanabe, K., *J. Catal.* **47,** 358 (1977).
51. Schreiber, L. B., and Vaughan, R. W., *J. Catal.* **40,** 226 (1975).
52. Johansen, P. G., and Buchanan, A. S., *Aust. J. Chem.* **10,** 398 (1957).
53. Parks, G. A., *Chem. Rev.* **65,** 177 (1965).
54. Millman, W. S., Segawa, K., Smrz, D., and Hall, W. K., *Polyhedron* **5,** 169 (1986).
55. Medema, J., van Stam, C., de Beer, V. H. J., Konings, A. J. A., and Koningsberger, D. C., *J. Catal.* **53,** 386 (1978).
56. Desikan, A. N., Huang, L., and Oyama, S. T., *J. Phys. Chem.* **95,** 10050 (1991).
57. Giordano, N., Bart, J. C. J., Vaghi, A., Castellan, A., and Martinotti, G., *J. Catal.* **36,** 81 (1975).
58. McMillan, M., Brinen, J. S., and Haller, G. L., *J. Catal.* **97,** 243 (1986).
59. Kasztelan, S., Payen, E., Toulhoat, H., Grimblot, J., and Bonnelle, J. P., *Polyhedron* **5,** 157 (1986).
60. Barthomeuf, D., *Zeolites* **10,** 131 (1990).
61. Glemser, O., and Wendlandt, H. G., *Angew. Chem.* **75,** 949 (1963).
62. Alwitt, R. S., *in* "Oxides and Oxide Films" (J. W. Diggle and A. K. Vijh, Eds.), Vol. 4, p. 169. Dekker, New York, 1976.